MATERIALS SCIENCES

Programmable droplet manipulation by a magnetic-actuated robot

An Li[1,2], Huizeng Li[1,2]*, Zheng Li[1,2], Zhipeng Zhao[1,2], Kaixuan Li[1,2], Mingzhu Li[1,2], Yanlin Song[1,2]*

Droplet manipulations are fundamental to numerous applications, such as water collection, medical diagnostics, and drug delivery. Structure-based liquid operations have been widely used both in nature and in artificial materials. However, current strategies depend mainly on fixed structures to realize unidirectional water movement, while multiple manipulation of droplets is still challenging. Here, we propose a magnetic-actuated robot with adjustable structures to achieve programmable multiple manipulations of droplets. The adjustable structure redistributes the resisting forces from the front and rear ends of the droplets, which determine the droplet behaviors. We can transport, split, release, and rotate the droplets using the robot. This robot is universally applicable for manipulation of various fluids in rough environments. These findings offer an efficient strategy for automated manipulation of droplets.

INTRODUCTION

Controllable manipulation of droplets is critical for a wide variety of applications (1–5), such as water collection and transportation (6), bioassay (7), and chemical reactions (8). Many plants and animals in nature manipulate droplets by exploiting their structures. Archetypal examples include cacti (9), spider silk (10), and the Namib Desert beetle (11), which collect and move water with conical spines, periodic spindle-knots, and convex bump structures, respectively. These asymmetric intrinsic structures induce a Laplace pressure gradient in the water droplets, causing the droplets to move in a preset direction (12, 13). Inspired by these strategies, various external forces, including electricity (14), magnets (4), acoustics (15), light (12), and wetting surfaces (16), are used to actuate droplets. Among them, magnetic force has the advantages of long-range action, safety, and easy control. Accordingly, many achievements have been reported to manipulate droplets using the magnetic force. For example, magnetic particles are used to drag water droplets on hydrophobic or wettability-patterned substrates (17, 18), and magnetically responsive materials are used to adjust the droplet wetting states for controllable droplet transportation (19–21).

Here, we report a facile and reliable method to achieve multiple manipulations of the droplet by a magnetic-actuated robot. This robot is prepared using a couple of steel beads in a programmable magnetic field. The structure of the robot, indicated by the ratio of the beads' center-to-center distance to the bead diameter, can be facilely adjusted by the magnetic field. Differentiated robot structures redistribute the resistive forces at the front and rear ends of the droplet, leading to diverse droplet behaviors including transport, split, release, rotation, and their combinations. The robot is universal to many kinds of fluids, including water, oil, and gas. It is actuated by a magnetic field, making it robust for use in limited spaces, on uneven surfaces, and even under anhydrous and anaerobic conditions. This method offers a facile strategy for programmable and automated manipulation of droplets, which shows great potential in various applica-

tions including material transportation, microfabrication, and clinical medicine.

RESULTS

The droplet manipulation system consists of two steel beads and a magnetic control system (Fig. 1A). Here, we name the two steel beads as the "robot" (22–24). The diameter of the beads is 1.2 mm, and the robot is actuated by a magnetic control system, as shown in fig. S1. We can design both the movement and the structure of the robot by the magnetic control system. The sequenced images in Fig. 1 (C to F) show the multiple droplet manipulations using the magnetic-actuated robot (movie S1). We color the water droplets with food dyes for distinction. Different droplet behaviors can be realized by adjusting the robot structure. Figure 1B displays the key parameters of the robot structure, including the diameter of the beads (d) and the distance between the beads (D). The robot is hydrophilic (the characterizations of the beads and the substrate are shown in fig. S2) and can easily capture the droplet after contact. We can transport the droplet using the robot with a proper structure (Fig. 1C). To split a daughter drop or release the droplet, we adjust the structure of the robot by reducing or increasing the distance between the beads (Fig. 1, D and E). Revolving the robot can facilely rotate the droplet, which greatly accelerates the material mixing in the droplet (Fig. 1E). Besides manipulating large water droplets (250 μl), we also realize the control of micro-drops with volume smaller than 10 μl (fig. S3).

The droplet manipulation processes mainly rely on the structure of the robot, while the volume of the droplet (V) will surely influence the manipulating results. To exhibit the droplet manipulation ability of the robot, we systematically investigate the dependence of the droplet behaviors on the robot structure and the droplet volume and summarize the results in Fig. 2A. Here, the structure of the robot is quantified by the ratio of the beads' center-to-center distance to the diameter (D/d), as shown in Fig. 2A. In general, droplet transport is achieved with moderate V and D/d; split of a daughter drop occurs when reducing D/d and enlarging V, while increasing D/d and/or V contributes to the release of the droplet from the robot. For example, the robot with a D/d of 1.67 can transport a 150-μl water droplet, while a daughter drop will be split and moved if the droplet volume

[1]Key Laboratory of Green Printing, CAS Research/Education Center for Excellence in Molecular Sciences, Institute of Chemistry, Chinese Academy of Sciences, Beijing 100190, P. R. China. [2]University of Chinese Academy of Sciences, Beijing 100049, P. R. China.
*Corresponding author. Email: ylsong@iccas.ac.cn (Y.S.); lhz1990@iccas.ac.cn (H.L.)
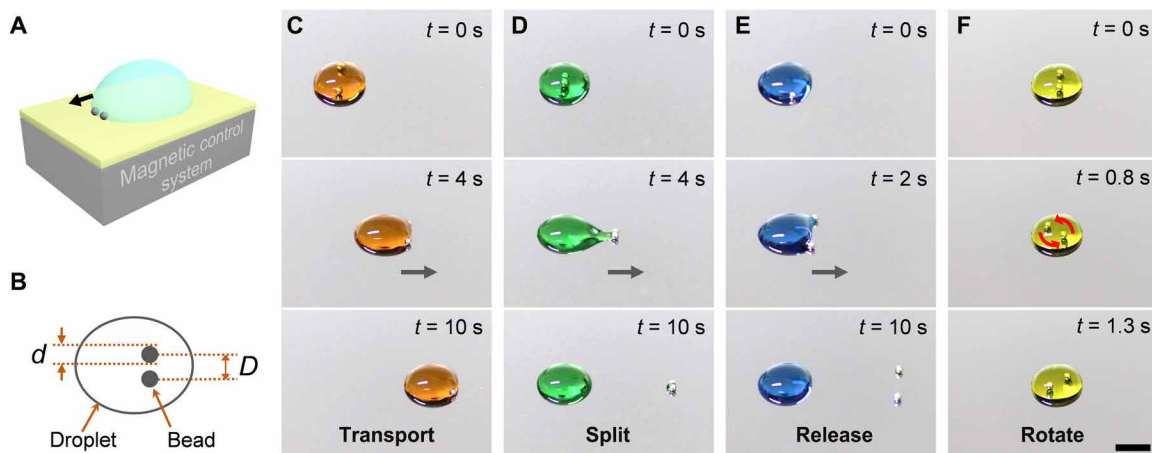
Fig. 1. Scheme and demonstration of the magnetic-actuated robot. (**A**) Scheme of the droplet manipulation system. (**B**) Parameters describing the magnetic-actuated robot. (**C** to **F**) Typical behaviors of the droplets manipulated by the robot. Droplets can be transported (C), split (D), released (E), and rotated (F) by the robot. The gray arrows represent the moving direction of the robots. The moving speed is 2 mm/s. The volume of the droplets is 250 μl. Scale bar, 5 mm.
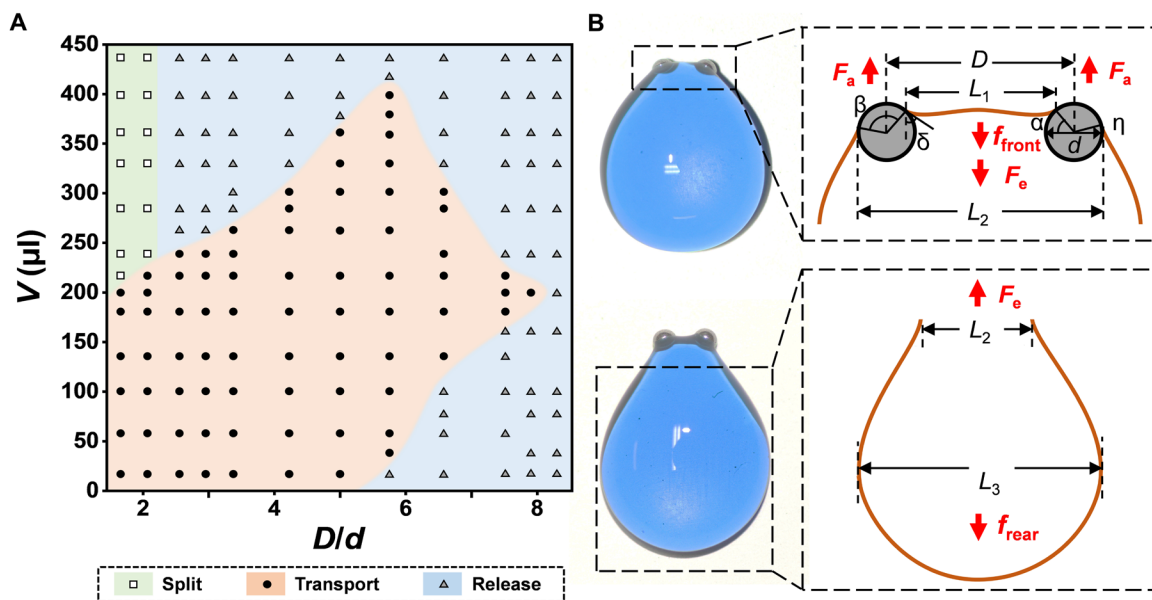

Fig. 2. Diagram and mechanical analysis of the droplet manipulation. (**A**) Phase diagram showing the diverse behaviors of the droplet with the variation of D/d and V. (**B**) Mechanical analysis explaining the actuating ability of the robot. Three forces, including the adhesion force between the liquid and the beads (F_a), the adhesion force between the liquid and the substrate (f_{front}), and the resilience force due to the deformation of the droplet (F_e), determine the movement of the TCL at the front end of the droplet (the upper scheme). Two main forces (F_e and f_{rear}) affect the movement of the TCL at the rear end of the droplet (the lower scheme).

enlarges to 350 μl. When increasing D/d to 3.33, the 350-μl droplet will be released by the robot, although the smaller droplet (150 μl) can still be transported (fig. S4 and movie S2).

To understand the origin of the diverse droplet behaviors performed by the robot, we conduct the mechanical analysis of this system, including the beads, the droplet, and the substrate, as shown in Fig. 2B. According to the droplet shape evolution (movie S1), the droplet behaviors are determined by the movement of the three-phase contact line (TCL) at the front end (the portion between the beads, as shown in Fig. 2B, top) and the rear end (Fig. 2B, bottom). Three forces decide the movement of the droplet at the front end.

The driving force is the adhesion force between the beads and the droplet (F_a); the resisting forces include the elastic force due to the droplet deformation (F_e) and the adhesion force between the droplet front end and the substrate (f_{front}) (25). The net force at the front end of the droplet is

$$F_{front} = 2F_a - F_e - f_{front} =$$
$$2 \oint \gamma \cos \delta \left(\pi d \cdot \sin \frac{\beta}{2} \right) dl - E \cdot \varepsilon \cdot A + \gamma \cos \theta_{adv} \cdot L_1 \quad (1)$$

where γ is the liquid surface tension; δ is the angle between the liquid and the moving direction (Fig. 2B); E is the elastic modulus of

the droplet; ε is the tension rate of the droplet, which is equal to the stretched length of the droplet to the maximum stretched length (26); l is the contour of the TCL around the bead; $A \approx d \cdot D$ is the cross-sectional area of the liquid between the beads; θ_{adv} is the advancing contact angle of the droplet on the substrate; and $L_1 = D - d \cos\alpha$. If the resisting force cannot be overcome by the driving force ($F_{front} \leq 0$), the TCL between the beads will be pinned, and the droplet will be released by the robot. Otherwise ($F_{front} > 0$), the front end will be pulled by the robot, and the droplet split or transport will occur, depending on the force balancing at the rear end. Two forces determine the movement of the rear end of the droplet: the driving force arising from the moving of the droplet front end (F_e) and the resisting force arising from the liquid-solid adhesion on the rear end (f_{rear}). The net force at the rear end (F_{rear}) is given by

$$F_{rear} = F_e - f_{rear} = E \cdot \varepsilon \cdot A - \gamma(\cos\theta_{rec} - \cos\theta_{adv})L_3 - \cos\theta_{adv}L_2 \quad (2)$$

where θ_{rec} is the receding contact angle of the droplet on the substrate, L_2 is the width of the thinnest liquid bridge behind the beads, and L_3 is the maximum width of the TCL contour between the droplet and the substrate. The droplet can be transported if the net force (F_{rear}) is positive; otherwise, a daughter drop will be split and transported. The detailed mechanical analysis and the phase diagram analysis are provided in sections S1 and S2. In addition, other factors, such as the droplet surface tension, the substrate fraction, and the size of the beads, also influence the droplet manipulation functions. Detailed analyses are shown in section S3.

Besides controlling the water droplet behaviors in the air, we systematically investigated the generality of the robot under different conditions (movie S3). Manipulation of oil or water drops under liquid environment is crucial to micro-organogel printing (27), soft robot fabrication (24), and emulsion reactions (28), especially because the reagents are sensitive to the atmospheric environment. After proper surface modification, the robot can be used to transport oil drops under water, move water drops under oil, and even collect gas bubbles under water. As shown in Fig. 3A, carbon tetrachloride (oil) droplets dissolved with bromine and styrene are placed under water. Dragged by the superhydrophobic beads, the two droplets approach and coalesce for the unsaturated bond detection (29). Similarly, a droplet of KSCN aqueous solution can be captured and moved by the superhydrophilic beads in an oil environment to react
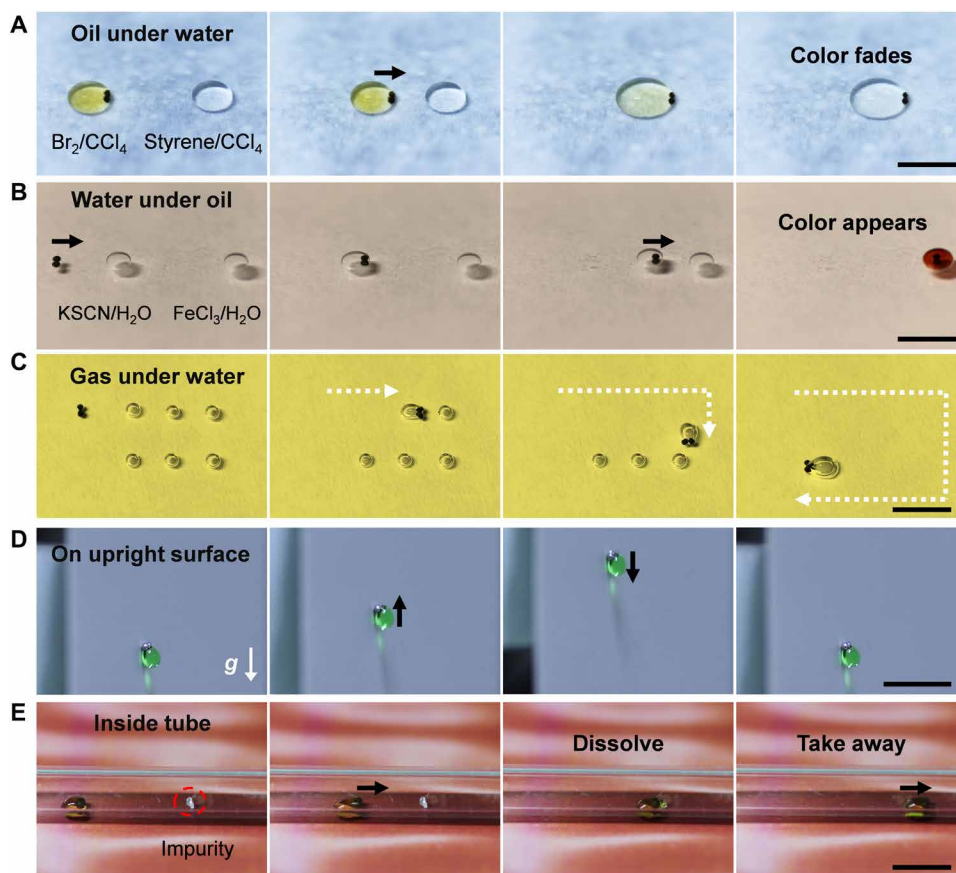

Fig. 3. Generality demonstration of the robot. (**A**) Oil droplet manipulation under water. The oil droplets (100 μl) are CCl₄-dissolved with Br₂ (left) and styrene (right). The robot transports the left droplet to mix with the right one. (**B**) Water droplet manipulation under oil (*n*-heptadecane). The droplets (50 μl) are water-dissolved with KSCN (left) and FeCl₃ (right), respectively. The left droplet is captured by the robot and transported to the right one. (**C**) Gas bubble manipulation under water. A superhydrophobic robot can successively collect the gas bubbles (20 μl). The white dotted line indicates the trajectory of the robot. (**D**) Manipulation of a water droplet on the upright surface. The robot transports a 20-μl water droplet to move up and down with a speed of 2 mm/s. (**E**) Manipulation of a water droplet inside a tube. A droplet (20 μl) is actuated by the robot to capture the impurity inside a tube. After 1 min, the impurity is dissolved and taken away by the droplet. The red dashed circle indicates the location of the impurity. The black arrow indicates the movement of the droplet. Scale bars, 10 mm.

with another aqueous droplet (Fig. 3B). In addition, Fig. 3C shows that the superhydrophobic robot can also successfully capture and collect gas bubbles distributed under water, which shows potential for removing bubbles in microfluidic devices (*30*). The key principle for specific surface modification of the robot is that the contact between the robot and the manipulated fluid (fluid-2) cannot be replaced by the contact between the robot and the bulk fluid (fluid-1). The quantitative judgment criterion for the effective surface modification is

$$\cos\alpha \ = \ \frac{\gamma_{1,s} - \gamma_{2,s}}{\gamma_{1,2}} \ > \ 0, \alpha \ < \ 90° \qquad (3)$$

where $\gamma_{1,s}$, $\gamma_{2,s}$, and $\gamma_{1,2}$ are the interface energies of the fluid-1/bead, fluid-2/bead, and fluid-1/fluid-2 interfaces and α is the contact angle. This means that if we intend to manipulate fluid-2 in the bulk fluid-1, the contact angle between fluid-2 and the bead should be smaller than 90° (see the detailed analysis in section S4).

Moreover, we demonstrate the applicability of the robot in rough environments, as most of the reported droplet manipulation methods become invalid because of the uneven surface or the limited operating space (*31*). Figure 3D displays the droplet manipulation on an upright surface. A colored water droplet can be dragged to move up and down by overcoming the gravity and adhesion force between the droplet and the substrate. The robot can also be applied in limited spaces, such as boxes and tubes, which is extremely important in microfluidics and clinical medicine (*30*). As shown in Fig. 3E, a tube is stained with impurities (NaCl) adhering to the tube. By manipulating

a droplet of water as the washing agent, the impurity can be easily dissolved and wiped off from the tube.

Lossless transport and precise control of reagents are notable in quantitative chemical reactions, especially in the micro-reaction, which is widely used in analytical chemistry, diagnostics, and biotechnology (*32*). For illustration, we perform sequential acid-base neutralization reactions through the programmable droplet manipulation using the robot, as shown in Fig. 4A. First, we split a daughter drop with a volume of 1.5 µl from a NaOH droplet (left) and transport it to a neutral phenolphthalein droplet (middle) by the robot with a proper structure of $D/d = 1.67$. The effect of the experimental parameters on the daughter drop volume is analyzed in section S5. After being merged and mixed with the daughter drop, the phenolphthalein droplet turns from colorless to pink, indicating that the solution is alkaline. Then, we take a tiny drop of HCl solution from a mother droplet (right) and mix it with the alkaline phenolphthalein droplet (middle). The color becomes colorless because of the neutralization reaction (movie S4). It is noteworthy that we can accelerate the mixing of liquid by rotating the droplet, and the quantitative mixing efficiency evaluation is shown in section S6. Our robot provides a versatile route to automatically control the droplets for micro-reactions, especially when the reagents are toxic, radioactive, or explosive. In fig. S6 and movie S5, we show that the toxic luminol reagent is prepared and manipulated by the robot for ferrum detection. (*33*).

Last, we explore the potential of the robot in in vivo medical applications by simulating typical biomedical processes. Calculi are minerals deposited in organs such as kidneys and gallbladders (*34*).
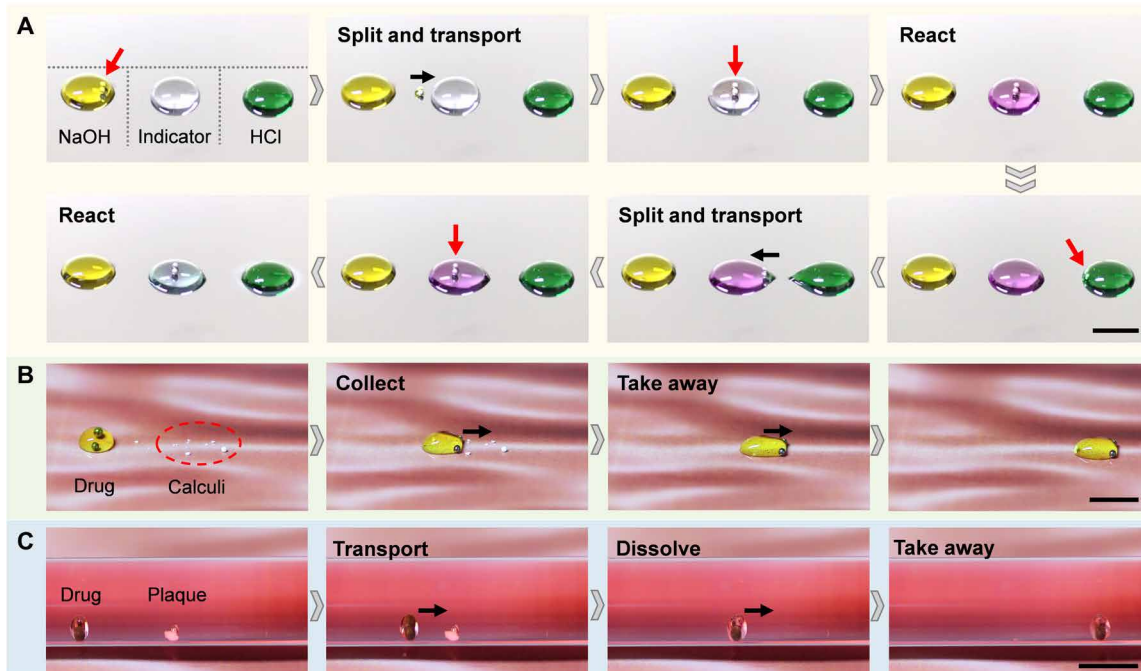

Fig. 4. Chemical and simulated medical applications using the robot. (**A**) Demonstration of stepwise chemical reactions. The robot split a daughter drop of 1.5 µl from a NaOH droplet and transport it to an indicator droplet (phenolphthalein). In the second step, the robot leaves the indicator droplet, splits a daughter drop from a HCl droplet, and then moves back to the indicator droplet. The volumes of the NaOH droplet, the indicator droplet, and the HCl droplet are all 250 µl. (**B**) Simulation of the calculi removal. The robot transports a droplet of drug to calculi placed on the substrate. The calculi are collected and taken away from the substrate. (**C**) Simulation of the vascular clearance. The drug droplet and the plaque placed inside a tube filled with water. The drug droplet is transported to the plaque by the robot. After 1 min, the plaque is dissolved and taken away. The black arrow indicates the movement of the droplet. The moving speed is 2 mm/s. Scale bars, 10 mm.

In clinical medicine, it is difficult to remove such structures surgically when their size is too small (*35*). In Fig. 4B, we show that the robot may be used to collect and remove the simulated calculi pieces. A drug droplet is dragged to the calculi that are randomly placed on the substrate. Because of the interface compatibility between the drug and the calculi, we can easily collect and take the calculi away from the substrate (movie S6). In addition, we demonstrate that the robot has potential for clearing the blood vessels. A surfeit of cholesterol can build up in coronary arteries and increase the chances of a stroke or heart attack (*36*). As shown in Fig. 4C, we use a tube filled with water to imitate the coronary arteries. The robot transports a drug droplet and captures the simulated plaque deposited inside the tube. After 1 min, the plaque is dissolved in the drug and is taken away by the robot. Furthermore, the demonstration of the drug delivery is given in fig. S7 and movie S8. These demonstrations may provide a new idea for in vivo medical applications (*22*, *37*).

DISCUSSION
We propose a simple and general strategy for manipulation of droplets by a magnetic-actuated robot made of two steel beads. We can control the structure of the robot by the magnetic field, which determines the distribution of the resistive forces at the front and rear ends of the droplet. Multiple behaviors of droplets, including transport, split, release, and rotation, are realized by adjusting the robot structure. In addition to manipulating water droplets in air, the robot is effective for complex liquid systems such as oil in water, water in oil, and gas in water. The robot can manipulate droplets in limited spaces, on inclined surfaces, and under harsh conditions such as toxic and radiative environments. It shows great potential in the fields of device fabrication, sensing and bioassay, and in vivo medical applications. In the future, smaller droplet manipulation (in the nano- or picoliter scale) and the biocompatibility of the system should be considered.

MATERIALS AND METHODS
Preparation of the magnetic-actuated robot
The magnetic-actuated robot consists of two components: a couple of steel beads and a magnetic control system. First, we placed two magnets on a motorized precise translation stage (stage I), which can control the distance between the magnets. Stage I is fixed on a rotary stage (stage II), which can control the magnets to rotate with adjustable speeds. Stage II is placed on a two-dimensional motorized precise translation stage that can drive the system to move in X/Y directions. Then, we placed a silicon plate on top of the magnets, and the steel beads were attracted by the magnets through the silicon plate. The cylindrical magnets are 5 mm in length and 1 mm in diameter. The intensities of the magnetic field on the surfaces of the magnet and the silicon plate are 150 and 25 mT, respectively. The diameter of the beads is 1.2 mm.

We prepared three kinds of beads with different surface modifications to manipulate the water droplets, the oil droplets, and the gas bubbles. The beads for the manipulation of water drops were washed by ethanol and deionized water, with a receding contact angle of 10.5 ± 1°, indicating that they are highly adhesive. Note that we used the steel sheets that are of the same material with the beads for the contact angle measurement. These beads were used for the experiments in Figs. 1 (C to F), 2B, 3D, and 4 (A and B). The beads

for water manipulation under oil, displayed in Fig. 3B, are superhydrophilic. To fabricate superhydrophilic beads, we first used the mixed solution of hydrochloric acid (40 ml), hydrofluoric acid (2.5 ml), and deionized water (12.5 ml) to etch the beads. Then, the beads were washed with ethanol, acetone, and deionized water and blow-dried with nitrogen. The beads for oil and gas manipulation under water, in Figs. 3 (A and C) and 4C, are superhydrophobic with a receding contact angle of 157.8° ± 3°. These beads were obtained by modification of the superhydrophilic beads with 1*H*,1*H*,2*H*,2*H*-perfluorodecyltrimethoxysilane (PFOTS) by chemical vapor deposition (CVD) at 80°C for 4 hours.

Preparation of the substrates
The hydrophobic substrates used in Figs. 1 (C to F), 3D, and 4A are silicon wafers modified with PFOTS by CVD at 80°C for 4 hours. The advancing and receding contact angles of these substrates were 115.5° ± 2° and 86.3° ± 2.8°, respectively. The test of oil droplet manipulation shown in Fig. 3A was carried out under water on commercial filter paper. The tests in Fig. 3 (B and C) were conducted in a polystyrene plastic dish. The substrate in Fig. 3E is a hydrophobic glass tube, which is pickled with sulfuric acid and H_2O_2 at 220°C for 6 hours and then modified with PFOTS by CVD at 80°C for 4 hours. The substrate in Fig. 4C is a superhydrophilic glass tube, which is pickled with sulfuric acid and H_2O_2 at 220°C for 6 hours.

Various chemical reactions
The droplets displayed in Figs. 1 (C to F), 2B, and 3 (D and E) are water droplets colored by edible dyes with a volume ratio of 1:100 (dye/water). In Fig. 4A, the NaOH droplet and the HCl droplet were colored by yellow and green edible dyes with a concentration of 1 M, respectively. The concentrations of the Br_2/CCl_4 and styrene/CCl_4 droplets in Fig. 3A are 0.1 M. In Fig. 3B, the concentrations of the $KSCN/H_2O$ and $FeCl_3/H_2O$ droplets are 0.1 M.

Simulated medical applications
The experiment of the simulated calculi removal, shown in Fig. 4B, was conducted on a polypropylene substrate. The simulated calculi are made of calcium carbonate. The drug droplet is a water droplet colored by yellow edible dyes with a volume ratio of 1:100 (dye/water). The volume of the drug droplet is 50 μl. The experiment of the vascular clearance was conducted in a glass tube (Fig. 4C). The tube was filled with water. The drug droplet is a CCl_4 droplet with a volume of 5 μl. The simulated plaque is a mixture of cholesterol and butter.

SUPPLEMENTARY MATERIALS

Movie S3. Generality demonstration of the magnetic-actuated robot.
Movie S4. Display of the stepwise acid-based neutralization reactions.
Movie S5. Display of the luminol reaction.
Movie S6. Simulation of the calculi removal.
Movie S7. Simulation of the drug delivery.
Movie S8. Simulation of the vascular clearance.

REFERENCES AND NOTES

1. J. V. I. Timonen, M. Latikka, L. Leibler, R. H. A. Ras, O. Ikkala, Switchable static and dynamic self-assembly of magnetic droplets on superhydrophobic surfaces. *Science* **341**, 253–257 (2013).

2. M. J. Fuerstman, P. Garstecki, G. M. Whitesides, Coding/decoding and reversibility of droplet trains in microfluidic networks. *Science* **315**, 828–832 (2007).

3. K. C. Park, P. Kim, A. Grinthal, N. He, D. Fox, J. C. Weaver, J. Aizenberg, Condensation on slippery asymmetric bumps. *Nature* **531**, 78–82 (2016).

4. W. Lei, G. Hou, M. Liu, Q. Rong, Y. Xu, Y. Tian, L. Jiang, High-speed transport of liquid droplets in magnetic tubular microactuators. *Sci. Adv.* **4**, eaau8767 (2018).

5. J. Li, Y. Hou, Y. Liu, C. Hao, M. Li, M. K. Chaudhury, S. Yao, Z. Wang, Directional transport of high-temperature Janus droplets mediated by structural topography. *Nat. Phys.* **12**, 606–612 (2016).

6. M. Damak, K. K. Varanasi, Electrostatically driven fog collection using space charge injection. *Sci. Adv.* **4**, eaao5323 (2018).

7. W. Feng, E. Ueda, P. A. Levkin, Droplet microarrays: From surface patterning to high-throughput applications. *Adv. Mater.* **30**, e1706111 (2018).

8. L. A. Bawazer, C. S. McNally, C. J. Empson, W. J. Marchant, T. P. Comyn, X. Niu, S. Cho, M. J. McPherson, B. P. Binks, A. deMello, F. C. Meldrum, Combinatorial microfluidic droplet engineering for biomimetic material synthesis. *Sci. Adv.* **2**, e1600567 (2016).

9. J. Ju, H. Bai, Y. Zheng, T. Zhao, R. Fang, L. Jiang, A multi-structural and multi-functional integrated fog collection system in cactus. *Nat. Commun.* **3**, 1247 (2012).

10. Y. Zheng, H. Bai, Z. Huang, X. Tian, F. Q. Nie, Y. Zhao, J. Zhai, L. Jiang, Directional water collection on wetted spider silk. *Nature* **463**, 640–643 (2010).

11. X. Yao, Y. Song, L. Jiang, Applications of bio-inspired special wettable surfaces. *Adv. Mater.* **23**, 719–734 (2011).

12. J. Lv, Y. Liu, J. Wei, E. Chen, L. Qin, Y. Yu, Photocontrol of fluid slugs in liquid crystal polymer microactuators. *Nature* **537**, 179–184 (2016).

13. M. Prakash, D. Quéré, J. W. M. Bush, Surface tension transport of prey by feeding shorebirds: The capillary ratchet. *Science* **320**, 931–934 (2008).

14. J. Li, N. S. Ha, T. L. Liu, R. M. van Dam, C. J. Kim, Ionic-surfactant-mediated electro-dewetting for digital microfluidics. *Nature* **572**, 507–510 (2019).

15. S. P. Zhang, J. Lata, C. Chen, J. Mai, F. Guo, Z. Tian, L. Ren, Z. Mao, P.-H. Huang, P. Li, S. Yang, T. J. Huang, Digital acoustofluidics enables contactless and programmable liquid handling. *Nat. Commun.* **9**, 2928 (2018).

16. S. Daniel, M. K. Chaudhury, J. C. Chen, Fast drop movements resulting from the phase change on a gradient surface. *Science* **291**, 633–636 (2001).

17. Z. Long, A. M. Shetty, M. J. Solomon, R. G. Larson, Fundamentals of magnet-actuated droplet manipulation on an open hydrophobic surface. *Lab Chip* **9**, 1567–1575 (2009).

18. Y. Zhang, T. H. Wang, Full-range magnetic manipulation of droplets via surface energy traps enables complex bioassays. *Adv. Mater.* **25**, 2903–2908 (2013).

19. D. Tian, N. Zhang, X. Zheng, G. Hou, Y. Tian, Y. Du, L. Jiang, S. X. Dou, Fast responsive and controllable liquid transport on a magnetic fluid/nanoarray composite interface. *ACS Nano* **10**, 6220–6226 (2016).

20. J. Belardi, N. Schorr, O. Prucker, J. Rühe, Artificial Cilia: Generation of magnetic actuators in microfluidic systems. *Adv. Funct. Mater.* **21**, 3314–3320 (2011).

21. S. Ben, T. Zhou, H. Ma, J. Yao, Y. Ning, D. Tian, K. Liu, L. Jiang, Multifunctional magnetocontrollable superwettable-microcilia surface for directional droplet manipulation. *Adv. Sci.* **6**, 1900834 (2019).

22. W. Hu, G. Z. Lum, M. Mastrangeli, M. Sitti, Small-scale soft-bodied robot with multimodal locomotion. *Nature* **554**, 81–85 (2018).

23. Y. Kim, G. A. Parada, S. Liu, X. Zhao, Ferromagnetic soft continuum robots. *Sci. Robot.* **4**, eaax7329 (2019).

24. H. Lu, M. Zhang, Y. Yang, Q. Huang, T. Fukuda, Z. Wang, Y. Shen, A bioinspired multilegged soft millirobot that functions in both dry and wet conditions. *Nat. Commun.* **9**, 3944 (2018).

25. N. Gao, F. Geyer, D. W. Pilat, S. Wooh, D. Vollmer, H.-J. Butt, R. Berger, How drops start sliding over solid surfaces. *Nat. Phys.* **14**, 191–196 (2017).

26. P. Chantelot, A. Mazloomi Moqaddam, A. Gauthier, S. S. Chikatamarla, C. Clanet, I. V. Karlin, D. Quéré, Water ring-bouncing on repellent singularities. *Soft Matter* **14**, 2227–2233 (2018).

27. C. S. O'Bryan, T. Bhattacharjee, S. Hart, C. P. Kabb, K. D. Schulze, I. Chilakala, B. S. Sumerlin, W. G. Sawyer, T. E. Angelini, Self-assembled micro-organogels for 3D printing silicone structures. *Sci. Adv.* **3**, e1602800 (2017).

28. Y. Zhao, J. Liu, Z. Chen, X. Zhu, M. Möller, Hybrid nanostructured particles via surfactant-free double miniemulsion polymerization. *Nat. Commun.* **9**, 1918 (2018).

29. B. Su, S. Wang, Y. Song, L. Jiang, Utilizing superhydrophilic materials to manipulate oil droplets arbitrarily in water. *Soft Matter* **7**, 5144–5149 (2011).

30. M. Prakash, N. Gershenfeld, Microfluidic bubble logic. *Science* **315**, 832–835 (2007).

31. L. Shang, Y. Cheng, Y. Zhao, Emerging droplet microfluidics. *Chem. Rev.* **117**, 7964–8040 (2017).

32. X. Tang, P. Zhu, Y. Tian, X. Zhou, T. Kong, L. Wang, Mechano-regulated surface for manipulating liquid droplets. *Nat. Commun.* **8**, 14831 (2017).

33. W. Gao, C. Wang, K. Muzyka, S. A. Kitte, J. Li, W. Zhang, G. Xu, Artemisinin-luminol chemiluminescence for forensic bloodstain detection using a smart phone as a detector. *Anal. Chem.* **89**, 6160–6165 (2017).

34. F. L. Coe, J. R. Asplin, Stopping the stones. *Science* **330**, 325–326 (2010).

35. S. R. Mulay, H. J. Anders, Crystal nephropathies: Mechanisms of crystal-induced kidney injury. *Nat. Rev. Nephrol.* **13**, 226–240 (2017).

36. C. M. Nielson, The root of all "bad" cholesterol. *Sci. Transl. Med.* **3**, 95ec126 (2011).

37. Y. Kim, H. Yuk, R. Zhao, S. A. Chester, X. Zhao, Printing ferromagnetic domains for untethered fast-transforming soft materials. *Nature* **558**, 274–279 (2018).